Applied Energy 261 (2020) 114426

Contents lists available at ScienceDirect

Applied Energy

journal homepage: www.elsevier.com/locate/apenergy

Optimal design of wind farms in complex terrains using computational fluid dynamics and adjoint methods

Enrico G.A. Antonini*, David A. Romero, Cristina H. Amon

University of Toronto, 27 King's College Circle, Toronto, Ontario M5S 1A1, Canada

HIGHLIGHTS

- The proposed adjoint method enables CFD-based wind farm design in complex terrains.
- The field-validated, turbulent CFD model predicts the wind farm energy generation.
- The developed CFD-based methodology optimally sites turbines over complex terrains.
- A full-scale CFD-based WFLO is completed in days using current computing resources.
- The energy generation of a real wind farm in complex terrain is increased by 6.6%.

ARTICLE INFO

Keywords:
Wind farm layout optimization
Complex terrain
CFD
RANS
Adjoint method
Gradient-based optimization

ABSTRACT

Optimal design of wind farms in complex terrains has never been fully addressed because of the complex flow phenomena generated by the turbine wakes, the terrain itself, and their mutual interaction. To capture these effects, Computational Fluid Dynamics (CFD) simulation models are necessary, but their direct use with traditional optimization algorithms is prevented by their high computational cost. By using a gradient-based algorithm and an adjoint method for the gradient calculations, we present a methodology for the optimization of wind farm layouts that enables the use of CFD models to accurately simulate wake effects and terrain-induced flow characteristics. As opposed to previous studies, this methodology is general in its formulation and can handle different wind farm configurations, wind resource distributions and terrain topography. Benefits of an optimal wind farm design that employs CFD models are demonstrated for idealized and real cases, where significant improvements in annual energy production are realized by optimally siting turbines over complex terrains exploiting both turbine- and terrain-induced flow features. We ultimately show that this innovative methodology is feasible with current computational resources and an optimization process can be completed within days.

1. Introduction

The siting of wind turbines when developing a new wind farm is a critical aspect in the design of these systems. Wind turbines, as they extract kinetic energy from the wind, create wakes that affect downstream turbines and can decrease the farm annual energy generation by 10–20% [1]. The process of finding the optimal position of wind turbines within an available terrain to maximize the energy production is called wind farm layout optimization (WFLO). It has become of great interest among wind farm designers and researchers as it has been shown that an optimal turbine arrangement can increase the overall energy generation [2] and diminish the wind farm levelized cost of electricity (LCOE) [3]. However, as more wind capacity is developed on-shore, both land use [4] and environmental impact [5] have become increasingly important constraints during the design process, thus stressing the importance of environmental [6] and public policy aspects [7] of the design of wind energy systems.

When wind farms are installed on-shore, a further problem usually arises: the terrain, when not flat, can have a significant impact on the local wind characteristics. Wind speed, direction and turbulence are all influenced by the local terrain topography [8], and this fact consequently impacts the wind farm operating conditions and performance. Studies of wind turbines and farms in complex terrain have been conducted both experimentally and numerically. Mattuella et al. [9] and Røkenes and Krogstad [10] analyzed in wind tunnel experiments the flow field over complex terrain for wind energy applications. They

* Corresponding author.
E-mail address: enrico.antonini@mail.utoronto.ca (E.G.A. Antonini).

https://doi.org/10.1016/j.apenergy.2019.114426
Received 23 October 2019; Received in revised form 17 December 2019; Accepted 18 December 2019

demonstrated how the wind characteristics significantly vary over the complex area creating speed-up regions, flow separation and steering. Numerical studies are more common as they are less expensive and time-consuming. They rely on Computational Fluid Dynamics (CFD) and the solution of the Navier–Stokes (N-S) equations to calculate the flow field and related quantities. Examples are given by Castellani et al. [11,12], Astolfi et al. [13], Murali and Rajagopalan [14], and Makridis and Chick [15]. A common feature of these numerical studies is that they include a validation phase in which the CFD models are assessed against field data, providing satisfactory agreement in most cases. All these experimental and numerical studies showed how the terrain changes and distorts the wind flow and underlined the necessity of an accurate characterization the flow regime in complex terrains. The WFLO problem, as discussed in the next paragraphs, has however been studied in vast majority for flat terrain applications with very few examples for complex terrains.

From a modelling viewpoint, an accurate estimation of the wind farm wake losses is crucial for the WFLO problem. To model wind turbine wakes, there exist two different approaches, namely analytical and numerical wake models [16]. Analytical models were developed from experimental and theoretical work on velocity deficit profiles and are generally simple and computationally inexpensive. The models developed by Jensen [17], Frandsen et al. [18], and Larsen [19] are among the most used. Ad hoc models are then needed to account for wakes overlapping in wind farm power calculations [20]: in such scenario, superposition of turbine wakes is assumed and complex flow phenomena neglected [21]. Because of the inherent simplifications, analytical wake models cannot resolve flow structures resulting from atmospheric processes, convective motions, speed-up effects surrounding turbine rotors or terrain features, variations in terrain roughness, and wake meandering [1]. By contrast, numerical models, which are based on CFD, are more accurate in resolving turbulent flows and provide a larger flexibility in handling different atmospheric conditions and terrain topography, albeit at a much larger computational cost. For wind farm simulations, there exist two distinct groups of CFD models, which have different approaches to model turbulence, namely Reynolds-Averaged Navier–Stokes (RANS) and Large-Eddy Simulation (LES) models [22]. RANS models are based on time-averaged N-S equations and necessitate additional modelling to calculate the resulting Reynolds stresses, whereas LES models are derived via a low-pass filtering on the N-S equations, where energy-containing eddies are resolved and smaller, dissipative eddies parametrized. RANS models are commonly used for wind farm simulations and are generally a robust tool for estimating the mean flow fields and power generation. The reader can refer to Ref. [22–27] for analyses and reviews of the RANS models in the context of wind farm simulations. LES models currently represent the simulation tool with the highest fidelity but they are still too computationally expensive for a design perspective. Mehta et al. [28] presented a comprehensive review about applications and additional details of wind farm LES.

The state of the art in WFLO is based on minimizing turbine wake losses calculated using analytical models [2,3,29]. This is because optimization frameworks that employ CFD models are computationally expensive and are generally constrained by computer resources. Metaheuristics and stochastic methods used to solve the WFLO problem include genetic/evolutionary algorithms (e.g., [7,4,30–34]), simulated annealing (e.g., [35]), particle swarms (e.g., [36–40]), and greedy algorithms (e.g., [41]). Other methods sometimes used to solve this problem are instead based on mathematical programming, which can be used independently (e.g., [42,43]) or combined with other heuristics (e.g., [44,45]). Nonlinear mathematical programming using exact gradients of the constraints and objective function has proved to be very efficient in tackling the WFLO problem and has been shown to outperform genetic algorithms in terms of computational cost and solution quality [46].

The usage of CFD-RANS models in WFLO, prevented originally by high computational costs, has been enabled partially by the advantage offered by mathematical programming. In fact, mathematical programming algorithms are characterized by a smaller number of simulations required to find an optimal solution [46]. The other key fact that has fully enabled the implementation of CFD-RANS models into the WFLO problem is the use of adjoints methods. The adjoint method is an efficient way for calculating the gradient of the objective function as required by continuous-variable optimization algorithms, particularly when the objective function depends on the solution of a system of state equations (e.g., the Navier–Stokes equations) [47]. When using adjoint methods, the total cost for the gradient calculation is independent of the number of design parameters and is comparable to that of a single CFD simulation. King et al. [48,49]and Antonini et al. [50] developed gradient-based approaches for WFLO that used an adjoint method in its discrete and continuous formulation, respectively. However, their implementations were for flat terrain configurations. Only two studies have focused on WFLO in complex terrain. Kuo et al. [51] developed a methodology that combines CFD with mixed-integer programming (MIP) to optimally site turbines on complex terrains. As a result of the proposed methodology and approximate initial solutions, they attained a favourable trade-off between solution quality and computational cost. Feng et al. [52] proposed instead an optimization framework that, to estimate the wake effects in complex terrain, used an analytical model superposed to a background field obtained through a CFD simulation. Even though full use of CFD models in the WFLO in complex terrain seems to be possible without any simplification, approximation or ad hoc solution, no example exists to date.

In the present paper, we present a methodology for the optimization of wind farm layouts that uses CFD models to accurately estimate wake effects and an adjoint method to calculate the gradients required by the gradient-based optimization. This methodology is general in its formulation and can handle any wind farm configurations, wind resource distributions and terrain topography. We show that a CFD-based methodology for wind farm layout optimization in complex terrain is feasible with current computational resources and an optimization process can be completed within days. First, we illustrate in Section 2 the adjoint method that we use for the gradient calculations, and we discuss its computational advantages with respect to traditional methods that originally prevented a successful implementation of a CFD-based wind farm layout optimization. In Section 3, we perform an important process for adjoint methods, that is the results verification. We run the verification process for an idealized 3D system by comparing the adjoint method with a central difference discretization method, expanding and complementing what was done by Antonini et al. [50] for 2D systems. In Section 4, we conduct a validation of the CFD model by comparing its predictions with publicly available, measured power production data from the Nygårdsfjellet wind farm. In Section 5, we present the WFLO methodology that combines the adjoint method and the CFD model to enable a full 3D, continuous-variable optimization of wind farms both in flat and complex terrains. We apply our methodology both to idealized cases and to the same real wind farm used for the validation. Results ultimately show the unique advantage of our methodology with respect the state of the art in WFLO, that is the capability of accurately simulating turbine wakes and terrain-induced flow features, and exploiting optimal turbine siting that approximate or simplified models could not provide. Conclusions, implications and potential impact of our study are then discussed in Section 6.

2. The adjoint method

In this section, we describe the general adjoint framework in its continuous formulation and discuss its computational advantages. For the detailed formulation of the adjoint method for the WFLO problem, the reader is referred to the work by Antonini et al. [50], who derived full 3D adjoint equations but demonstrated a 2D implementation valid only in flat terrains. After presenting the general mathematical

framework, as first conceptualized by Jameson [53], we discuss the specific modifications required to apply the formulation presented in Ref. [50] to complex terrains.

The governing equations of the present problem can be expressed as $\boldsymbol{G}(\boldsymbol{\phi}, \boldsymbol{\alpha}) = 0$, where $\boldsymbol{G}$ is the vector of the state equations (the RANS equations for the CFD-based WFLO), $\boldsymbol{\phi}$ is the vector of the flow field variables (the state variables in adjoint terminology), and $\boldsymbol{\alpha}$ is the vector including the wind turbine positions (the design variables). The system of the governing equations inherently relates the state variables, $\boldsymbol{\phi}$, to the design variables, $\boldsymbol{\alpha}$. An objective or cost function in scalar form that measures a quantity of interest (the total energy or power generation of the farm) is then defined as the integral of a user-defined function, $J[\boldsymbol{\phi}(\boldsymbol{\alpha}), \boldsymbol{\alpha}]$, over a given domain, Ω_O. The objective of such defined optimization problem is to find within certain constraints the optimal design variables that maximize the objective function, which can be expressed in formulas as:

$$\begin{aligned} \max_{\boldsymbol{\alpha}} \quad & \int_{\Omega_O} J[\boldsymbol{\phi}(\boldsymbol{\alpha}), \boldsymbol{\alpha}] d\Omega, \\ \text{subject to} \quad & \boldsymbol{G}[\boldsymbol{\phi}(\boldsymbol{\alpha}), \boldsymbol{\alpha}] = 0 \quad \text{in } \Omega, \\ & k(\boldsymbol{\alpha}) = 0, \\ & h(\boldsymbol{\alpha}) \leqslant 0, \end{aligned} \tag{1}$$

where Ω is the system domain, and k and h are equality and inequality constraints, placed on the design variables $\boldsymbol{\alpha}$ and defined *a priori* by the user. In the WFLO problem, these constraints typically represent wind farm site boundaries and wind turbines interspacing.

The solution of the above optimization system with gradient-based methods requires the objective function gradient with respect to the design variables, i.e., $d\left(\int_{\Omega_O} J d\Omega\right)/d\boldsymbol{\alpha}$. Within the adjoint framework, an expression for this gradient can be derived by introducing the Lagrangian function:

$$L = \int_{\Omega_O} J d\Omega + \int_{\Omega} \hat{\boldsymbol{\phi}}^T \boldsymbol{G} d\Omega, \tag{2}$$

where $\hat{\boldsymbol{\phi}}$ is the vector of the adjoint variables (also known as Lagrange multipliers). The fact that $\boldsymbol{G}$ is zero by construction implies that the objective function and its variation are equal to the Lagrangian and its variation (i.e., $J = L$ and $\delta\left(\int_{\Omega_O} J d\Omega\right) = \delta L$). The focus will then be placed on finding a convenient expression of the Lagrangian variation. The adjoint variables, $\hat{\boldsymbol{\phi}}$, on the other hand, can be freely chosen. Using the chain rule, the variation of the Lagrangian is expressed as:

$$\begin{aligned} \delta L = & \frac{\partial}{\partial \boldsymbol{\alpha}}\left(\int_{\Omega_O} J d\Omega\right)\delta\boldsymbol{\alpha} + \frac{\partial}{\partial \boldsymbol{\alpha}}\left(\int_{\Omega} \hat{\boldsymbol{\phi}}^T \boldsymbol{G} d\Omega\right)\delta\boldsymbol{\alpha} + \\ & + \int_{\Omega_O}\left(\frac{\partial J}{\partial \boldsymbol{\phi}} + \hat{\boldsymbol{\phi}}^T \frac{\partial \boldsymbol{G}}{\partial \boldsymbol{\phi}}\right)\frac{d\boldsymbol{\phi}}{d\boldsymbol{\alpha}}\delta\boldsymbol{\alpha} d\Omega + \int_{\Omega \setminus \Omega_O}\left(\hat{\boldsymbol{\phi}}^T \frac{\partial \boldsymbol{G}}{\partial \boldsymbol{\phi}}\right)\frac{d\boldsymbol{\phi}}{d\boldsymbol{\alpha}}\delta\boldsymbol{\alpha} d\Omega. \end{aligned} \tag{3}$$

Among all the terms in Lagrangian variation, the partial derivatives of the objective function with respect to the state variables, $\partial J/\partial \boldsymbol{\phi}$, and design variables, $\partial\left(\int_{\Omega_O} J d\Omega\right)/\partial\boldsymbol{\alpha}$, are straightforward to determine because the objective function is user-defined. The partial derivative of the state equations with respect to the state variables, $\partial \boldsymbol{G}/\partial\boldsymbol{\phi}$, can be obtained using common derivation rules. The partial derivative of the state equations with respect to the design variables, $\partial\left(\int_{\Omega} \hat{\boldsymbol{\phi}}^T \boldsymbol{G} d\Omega\right)/\partial\boldsymbol{\alpha}$, is generally zero, but it was shown in Ref. [50] that, for the WFLO formulation, this term is not equal to zero and requires special treatment. In fact, when the volumetric source terms in the state equations depend on the design variables, this term accounts for the source position variation and for the subsequent imbalance in the state equations.

With respect to the original formulation that was implemented for 2D systems [50], a geometric modification to the gradient calculation needs to be introduced when the terrain is not flat. In this case, the gradient is computed on an inclined plane tangential to the terrain at the turbine position. Of that gradient, only the projection on a horizontal plane has to be considered, as the design variables are expressed as planar coordinates. The practical consequence to this modification is that any position shift and its induced state equation imbalance, as discussed in the previous paragraph, must occur on such inclined plane.

For high-dimensional problems, $d\boldsymbol{\phi}/d\boldsymbol{\alpha}$ is perhaps the most computationally expensive term, but its calculation can be avoided by selecting the adjoint variables such that:

$$\begin{aligned} & \frac{\partial J}{\partial \boldsymbol{\phi}} + \hat{\boldsymbol{\phi}}^T \frac{\partial \boldsymbol{G}}{\partial \boldsymbol{\phi}} = 0 \qquad \text{in } \Omega_O, \\ & \hat{\boldsymbol{\phi}}^T \frac{\partial \boldsymbol{G}}{\partial \boldsymbol{\phi}} = 0 \qquad \text{in } \Omega \setminus \Omega_O. \end{aligned} \tag{4}$$

This is the system of adjoint equations and can be solved in a computational time that is similar to the solution of the system of state equations. With appropriate values for the adjoint variables, the total gradient required by the optimization algorithm is therefore:

$$\frac{d}{d\boldsymbol{\alpha}}\left(\int_{\Omega_O} J d\Omega\right) = \frac{dL}{d\boldsymbol{\alpha}} = \frac{\partial}{\partial\boldsymbol{\alpha}}\left(\int_{\Omega_O} J d\Omega\right) + \frac{\partial}{\partial\boldsymbol{\alpha}}\left(\int_{\Omega} \hat{\boldsymbol{\phi}}^T \boldsymbol{G} d\Omega\right). \tag{5}$$

The derivation of the partial derivative terms discussed above can be found in Ref. [50]. In the current methodology, the adjoint equations for turbulent flows with the $\kappa - \omega$ turbulence model are used.

3. Verification of the adjoint method

In this section, we verify the accuracy of the gradient calculated with the adjoint method in 3D systems by comparing its predictions with a finite difference discretization, defined as:

$$\frac{d}{d\boldsymbol{\alpha}}\left(\int_{\Omega_O} J d\Omega\right) = \frac{\int_{\Omega_O} J(\alpha_n + \delta\alpha_n) d\Omega - \int_{\Omega_O} J(\alpha_n - \delta\alpha_n) d\Omega}{2\delta\alpha_n} \quad n = 1, \ldots, N, \tag{6}$$

where $\delta\alpha_n$ is a perturbation of the n-th design variable. The central difference approach, differently from the adjoint method, needs two objective function evaluations for each design variable, and therefore it is $2N$ times more computationally expensive. This form of verification is common for assessing the accuracy of the gradient (e.g., [54–57]). The same approach was also used by Antonini et al. [50] for the verification of their 2D implementation of the adjoint method. We conducted the comparison by defining the idealized 3D verification case shown in Fig. 1 where we considered as quantity of interest the power generation of a wind turbine operating in wake conditions. We defined a regular grid of downstream and cross-stream positions where the gradient of the power generation was evaluated with respect to the two planar coordinates, resulting in a streamwise and a lateral component. The positions of the second turbine were set to $4D$ and $6D$ downstream, with a lateral spacing of $0.5D$, where D is the turbine rotor diameter equal to 80 m.

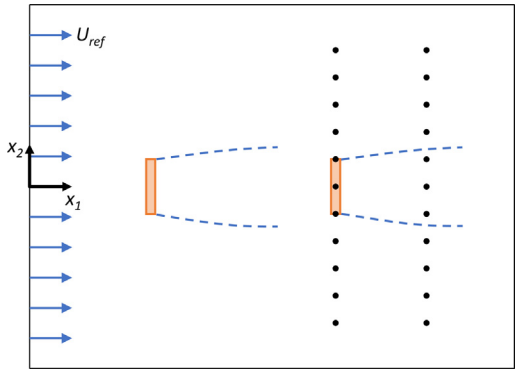

Fig. 1. Illustration of the verification case. The two orange-colored rectangles indicate the regions where the momentum sources representing the turbines are applied. The second turbine is progressively placed at different locations, indicated by the black dots, where the gradients are calculated. (For interpretation of the references to colour in this figure legend, the reader is referred to the web version of this article.)

The wind turbines were implemented as actuator disks, where a distributed axial momentum source is applied over a cylindrical region, determined by the turbine rotor area. The domain had dimensions of $10 \times 14 \times 6\ D$ with a global grid resolution of $0.1\ D$. A resolution of $0.05\ D$ was used in a refined region surrounding the wind turbines to accurately resolve the most significant gradients in the flow field. Near the terrain, the height of the first grid cell at the wall was set to $0.01D$, progressively increased for the neighboring cells moving away from the wall, up to the size given by the global resolution. The near-wall mesh refinement occurred within a height of $0.5D$. Second-order discretization was used for the primal and adjoint equations to interpolate the flow and adjoint variables. The semi-implicit method for pressure-linked equations (SIMPLE) algorithm was used to solve iteratively the set of equations, as implemented in OpenFOAM [58]. This numerical setup is consistent with previous studies about wind farm simulations, such as the ones in Ref. [24,26,59,60].

The boundary conditions for the primal, CFD simulations were set with realistic, typical values for the wind speed and turbulence quantities, whose profiles can be found in Ref. [26]. Assuming the atmospheric boundary layer characteristics, i.e., undisturbed wind speed, $U_{ref} = 10$ m/s, at reference height, $H = 60$ m, and surface roughness, $z_0 = 0.0018$ m, the profiles of wind speed, turbulence kinetic energy, k, and specific dissipation rate, ω, were specified at the inlet. The side and outlet boundary conditions were set as zero gradient and pressure outlet, respectively. The boundary conditions for the adjoint variables were instead defined according to the following equations [50]:

$$\begin{aligned} \hat{v}_i &= 0 \quad \text{in } \Gamma, \\ \frac{\partial \hat{p}}{\partial x_i} &= 0 \quad \text{in } \Gamma, \\ \hat{k} &= 0 \quad \text{in } \Gamma, \\ \hat{\omega} &= 0 \quad \text{in } \Gamma. \end{aligned} \tag{7}$$

We compared the results of the adjoint method (AM) with those of a central difference (CD) approach, which can be view as the best approximation for gradient calculations when analytical values are not available. Fig. 2 displays the values of the gradient components calculated by the adjoint and CD approaches whereas evaluation metrics are reported in Table 1. These metrics are: the relative magnitude of the gradient calculated with the adjoint method:

$$\|\nabla J_{rel}\| = \frac{\|\nabla J_{AM}\|}{\|\nabla J_{AM,max}\|} \cdot 100; \tag{8}$$

the percentage difference in the absolute value of the gradients calculated by the adjoint method with respect to the central difference discretization:

Table 1
Relative magnitude of the gradient calculated with the adjoint method, $\|\nabla J_{rel}\|$, and errors in absolute value, $\text{err}_{\nabla J}$, and direction, err_{θ}, between the gradient computed with the adjoint method and the central difference approach on the grid of downstream locations.

	4D downstream			6D downstream		
Cross-stream [D]	$\|\nabla J_{rel}\|$ [%]	$\text{err}_{\nabla J}$ [%]	err_{θ} [°]	$\|\nabla J_{rel}\|$ [%]	$\text{err}_{\nabla J}$ [%]	err_{θ} [°]
0.0	19.4	1.2	0.0	10.9	4.1	0.0
0.5	100.0	1.2	0.7	63.6	1.3	1.3
1.0	99.3	7.1	2.2	75.7	1.9	2.4
1.5	21.5	1.0	19.5	27.4	1.1	14.4
2.0	6.9	4.7	91.4	7.6	3.6	71.6
2.5	6.5	5.4	118.7	6.6	5.7	123.6

$$\text{err}_{\nabla J} = \frac{\|\nabla J_{AM}\| - \|\nabla J_{CD}\|}{\|\nabla J_{CD,max}\|} \cdot 100; \tag{9}$$

the angular difference in the direction between the gradient computed with the adjoint method and the central difference discretization:

$$\text{err}_{\theta} = \|\theta_{AM} - \theta_{CD}\|. \tag{10}$$

The adjoint method had predictions that were overall accurate for most part of wake region with the largest discrepancy of just 5.7% in the absolute value. High discrepancies in the gradient direction can instead be observed when the second turbine was in the outermost positions. This is explainable by considering that the two components of the gradient had a value close to zero, and even a minimal discrepancy in one of the two can result in a large direction variation. In these positions, the absolute value of the gradient is however smaller and almost negligible with respect to the wake region, and consequently this effect is not expected to have an impact on the optimization process. Overall, the validation results of the continuous adjoint method for 3D simulations are consistent with those obtained for 2D simulations [50] and provide the same significant saving in computational time, as discussed in Section 2. The successful verification of the 3D formulation of the adjoint method enables its application to any kind of 3D system and therefore it will be implemented in the optimization methodology for complex terrains.

4. Validation of the CFD model

To enable a reliable use of CFD models for predicting flow-dependent variables, a validation against experimental data is always

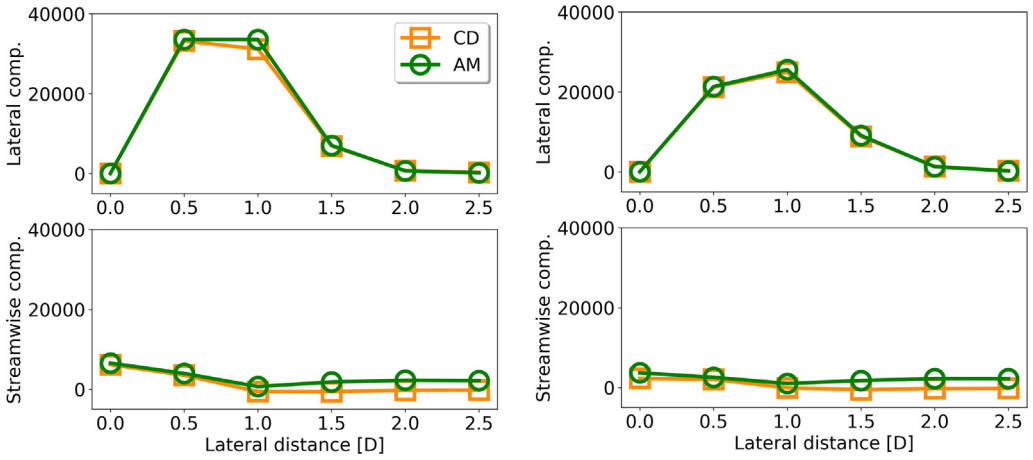

(a) 4D downstream (b) 6D downstream

Fig. 2. Gradient components. The figures display results obtained by the adjoint method (AM) and a central difference (CD) discretization approach for the different lateral positions of the second wind turbine at 4 D (a) and 6 D downstream (b).

recommended. In this paper, we propose a methodology for the optimization of turbine layouts that uses full-scale, 3D CFD models to predict the annual energy production of a wind farm. Hence, a validation of the CFD model predictive accuracy is of critical importance. In this section, we conduct the validation of the CFD model by comparing its predictions with observed power production values in an actual wind farm for which there is openly available production data.

The wind farm in consideration is the Nygårdsfjellet facility, located in Narvik, Norway. It consists of 14 Siemens SWT-2.3-93 wind turbines with a rated power of 2.3 MW each. They have a rotor diameter of 93 m and a hub height of 80 m with base foundations at 420 m above mean sea level. The wind farm is sited on a moderately complex terrain with smooth hills and on a terrain covered mainly in grass interrupted by small lakes. A measuring campaign was conducted at the wind farm site by collecting wind speed and direction from two anemometers placed on the nacelle as well as power production [61]. Even though model validations in complex terrains still remain a challenge for the lack of comprehensive data sets and high uncertainties, this campaign offers sufficient measurements for a comparison and details of the wind farm site and turbines.

We developed a CFD model based on RANS equations for incompressible, steady flows, which require additional turbulence modeling to solve the nonlinear Reynolds stress term. Here we used the standard $k-\omega$ model formulated by Wilcox [62], which relies on the Boussinesq approximation to calculate the Reynold stresses. Application-specific turbulence model constants were chosen as proposed by Antonini et al. [25,26]. This choice of turbulence model was motivated by the consistency with respect to the adjoint method formulation and by the sufficiently accurate predictions that this model can provide in wind farm simulations [27,59]. The domain had dimensions of $25 \times 25 \times 8$ D, whereas the mesh resolution was derived in a similar way as discussed in Section 3, resulting in a total of approximately 8 million cells. The terrain altitude was retrieved from Google Earth considering an area of 6×6 km^2 (roughly 64×64 D) centered at geographic coordinates 17.8821° E, 68.5074° N (effects of Earth's curvature were neglected). The terrain geometry and the turbine positions are illustrated in Fig. 3. OpenFOAM [58] is employed to solve the RANS equations, using a control-volume-based technique to transform the governing flow equations into algebraic expressions that can be solved numerically. Consistently with the adjoint formulation, second-order discretization was used for RANS equations and the SIMPLE algorithm was employed to solve the set of equations.

In order to validate the CFD model, we compared its predictions with power production measurements of wind turbines operating in wake conditions. Specifically, we considered the following eight cases

Table 2
Cases used for the validation of the CFD model. The freestream wind speed was 9 m/s for each of them, whereas the wind direction that corresponds to the condition of alignment between the two wind turbines in consideration and the wind speed is reported in the second column of the table.

Case	Wind direction [°]
5 in the wake of 1	271.2
6 in the wake of 2	279.3
6 in the wake of 12	93.6
7 in the wake of 3	283.3
7 in the wake of 11	93.4
8 in the wake of 10	74.7
9 in the wake of 10	95.2
14 in the wake of 4	270.0

whose field data are reported in Ref. [61]: turbine 5 operating in the wake of 1, 6 in the wake of 2, 6 in the wake of 12, 7 in the wake of 3, 7 in the wake of 11, 8 in the wake of 10, 9 in the wake of 10, and 14 in the wake of 4. For these cases, the freestream wind speed was of 9 m/s. The elevation of the freestream wind speed was reasonably assumed to be the average altitude of all the turbine hub heights, which was 210 m above the lowest point in the domain (130 m was the average elevation of the turbine bases). The wind direction that corresponds to the condition of alignment between the two wind turbines in consideration and the wind speed is reported in Table 2. For computational convenience, we rotated the wind farm layout and the underlying terrain according to the specified wind direction as opposed to rotating the boundary conditions. The boundary conditions were instead kept fixed as illustrated in Fig. 4. Assuming a terrain roughness of $z_0 = 0.0018$ m typical of grass land and neutral atmospheric conditions, the inlet boundary condition of the simulation was specified using a logarithmic profile for the wind speed, constant value for the turbulence kinetic energy, k, and hyperbolic profile for the specific dissipation rate, ω. More details of these profiles and their equations can be found in Ref. [26]. The side and outlet boundary conditions were set as zero gradient and pressure outlet, respectively.

Results from the validation procedure are reported in Fig. 5. Each subplot shows the observed normalized power along with one standard deviation and the CFD predictions as a function of wind direction for each of the cases considered. Several observations can be made from an analysis of the results. The first and most important is related to the field data: high uncertainties can be observed for most of the experimental data, with values of the standard deviation that can be as high as 40% of the normalized power. These uncertainties are the result of the

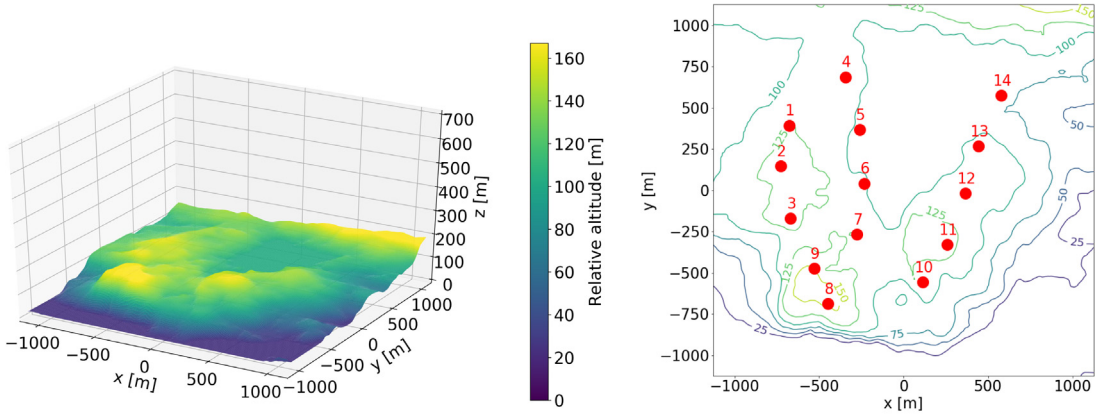

(a) Terrain geometry (b) Turbine positions

Fig. 3. Illustration of wind farm terrain and layout. The planar coordinates are centered at geographic coordinates 17.8821° E, 68.5074° N. The altitude is instead reported with respect to the lowest altitude of the area considered.

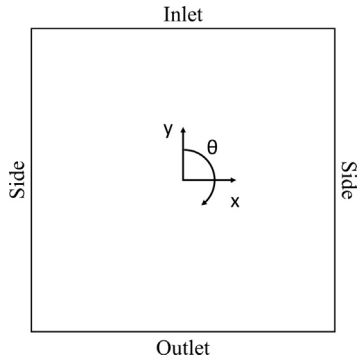

Fig. 4. Schematic of the domain, boundary conditions, and wind farm rotation strategy adopted in the simulations.

high variability of wind speed and direction, which is also increased by the terrain features that distort the wind flow. The effect of the terrain can be seen particularly on the profile of the normalized power as a function of wind direction. On flat terrains, its profile is usually symmetric about the direction for which the turbines are aligned with the incoming wind speed. However, the results show a clear asymmetry especially for the cases where the wind comes from the east sector. To note is also the fact that for the same cases, the normalized power is greater than unity for some wind directions, suggesting that the downstream wind turbines face a higher wind potential as a consequence of flow-distorting effects caused by the terrain. As pointed out by Seim et al. [61], yaw misalignment that occurs under varying wind conditions contributes both to the uncertainty and the normalized power greater than unity.

With regard to the CFD predictions, a good agreement can be observed in most of the cases, even though, for some wind directions, the discrepancies with observations are significantly large. For the first six cases of Fig. 5, the CFD model was able to capture the profile of normalized power, the wake width, and the wake centerline. The highest discrepancies are instead observed for the last two cases where the CFD model was likely not able to correctly simulate flow distortions caused by terrain features. A few reasons for these discrepancies can be reasonably identified. First, the domain of the CFD model was likely not extended enough to capture all the terrain features that generated the flow distortion. To have a more accurate capture of the flow field with all terrain-induced features, a much larger domain extending for a few kilometers upwind would have been necessary to allow the flow to fully develop. We however deemed this solution to be not computationally feasible for the subsequent optimization procedure. We, in fact, chose a domain size that was enough to capture a significant area surrounding the wind farm but whose solution could be achieved within our computational constrains. These constrains were given as two hours of simulation time with 120 Intel "Skylake" cores at 2.4 GHz. The second reason is likely related to the choice of turbulence model. Even though the $k-\omega$ model was chosen because of consistency with respect to the adjoint method and sufficiently accurate predictions in previous studies, it is not the most accurate when compared to more advance turbulence models, such as the $SSTk-\omega$ model [26]. The third reason is likely related to the altitude and location of the freestream wind speed that we assumed in our simulations. We used the most reasonable values but we are aware that, given the terrain geometry and the distance between the domain boundaries and the wind turbine positions where the measurements were taken, we may have introduced a systematic error. Other reasons for the discrepancies may be related to atmospheric stratification, not accounted for in the simulations, and yaw misalignment, not modeled.

Overall, our CFD model was able to provide good predictions of the power production for most of the wind directions considered but failed in a few of them. The validation process can be considered satisfactory but also highlighted the challenge of simulating wind farms in complex terrains. A comprehensive validation with more accurate predictions would have required larger domains and more powerful computational resources. This was however beyond the scope of the present paper where we instead want to show the feasibility of the first CFD-based wind farm optimization in complex terrain that can be done within days, or more precisely, with a computational budget of approximately 1000 core-days.

5. Wind farm layout optimization in complex terrains

The annual energy production (AEP) calculated with the CFD model and the gradient computation performed with the adjoint method are fundamental parts of the optimization methodology developed in this study, which is an extension of the one developed by Antonini et al. [50]. As opposed to the original implementation, the present methodology is developed to handle 3D systems and any kind of terrain. The goal of this methodology is to optimally site any given number of wind turbines within an available land and on any terrain geometry to maximize the AEP. As shown in Fig. 6, it requires the wind rose, i.e., the frequency distribution of the wind directions and speeds at the wind farm site; an initial, hypothetical wind farm layout; and the terrain geometry. First, CFD simulations are employed to estimate the AEP of a given layout. Adjoint simulations are then performed to calculate the gradient of the objective function, i.e., the variation of the AEP with respect to a variation in the turbine positions. With the computed gradients, turbine positions are updated and a new layout is assessed with additional CFD simulations. The above described steps are repeated until the user-provided termination criteria are satisfied. A gradient-based optimizer controls the processes of monitoring the convergence and updating the turbine positions. Here we used the sequential quadratic programming (SQP) algorithm part of the open-source library NLopt [63,64]. Convergence is considered reached when an improvement in the AEP of the new layout is less than 0.01%.

This methodology was applied and tested on two wind farms in complex terrain. The first one is an idealized wind farm consisting of 5 wind turbines, which provides useful heuristics for checking optimization results, and the second is the Nygårdsfjellet wind farm, used for the validation is Section 4.

5.1. Idealized wind farm

For the 5-turbine idealized wind farm, we defined a domain with dimensions of $12 \times 12 \times 6\ D$ and a circular region with a $3\ D$ radius inside which turbines could be placed. A minimum interspacing of $1\ D$ between wind turbines was also enforced to prevent any wind turbine superposition generated by the optimizer. The terrains used to test the optimization were of two kinds, flat and complex. For the complex terrain, we defined a Gaussian-shaped hill in the middle of the domain, whose geometry is given by the following expression:

$$z(x,y) = H\exp\left\{-\left[\frac{(x-x_0)^2}{2\sigma^2} + \frac{(y-y_0)^2}{2\sigma^2}\right]\right\}, \tag{11}$$

where H is the maximum height of the hill, σ is a parameter that determines the spread of the hill (akin to the standard deviation of the Gaussian distribution), and x_0 and y_0 are the coordinates of the maximum height of the hill. For the present case, the height and the standard deviation were set to $0.5D$ and $1D$, respectively. To highlight the advantages of the present methodology for 3D systems, this was also compared to the methodology developed for 2D systems in Ref. [50] for the same initial configurations and boundary conditions. As such, we had in total three different domains, as shown in Fig. 7. Lastly, to examine the dependence of the gradient-based framework on the initial conditions, we tested two initial layouts, one regular and one random (see Fig. 8). The wind rose used to characterize the wind distribution

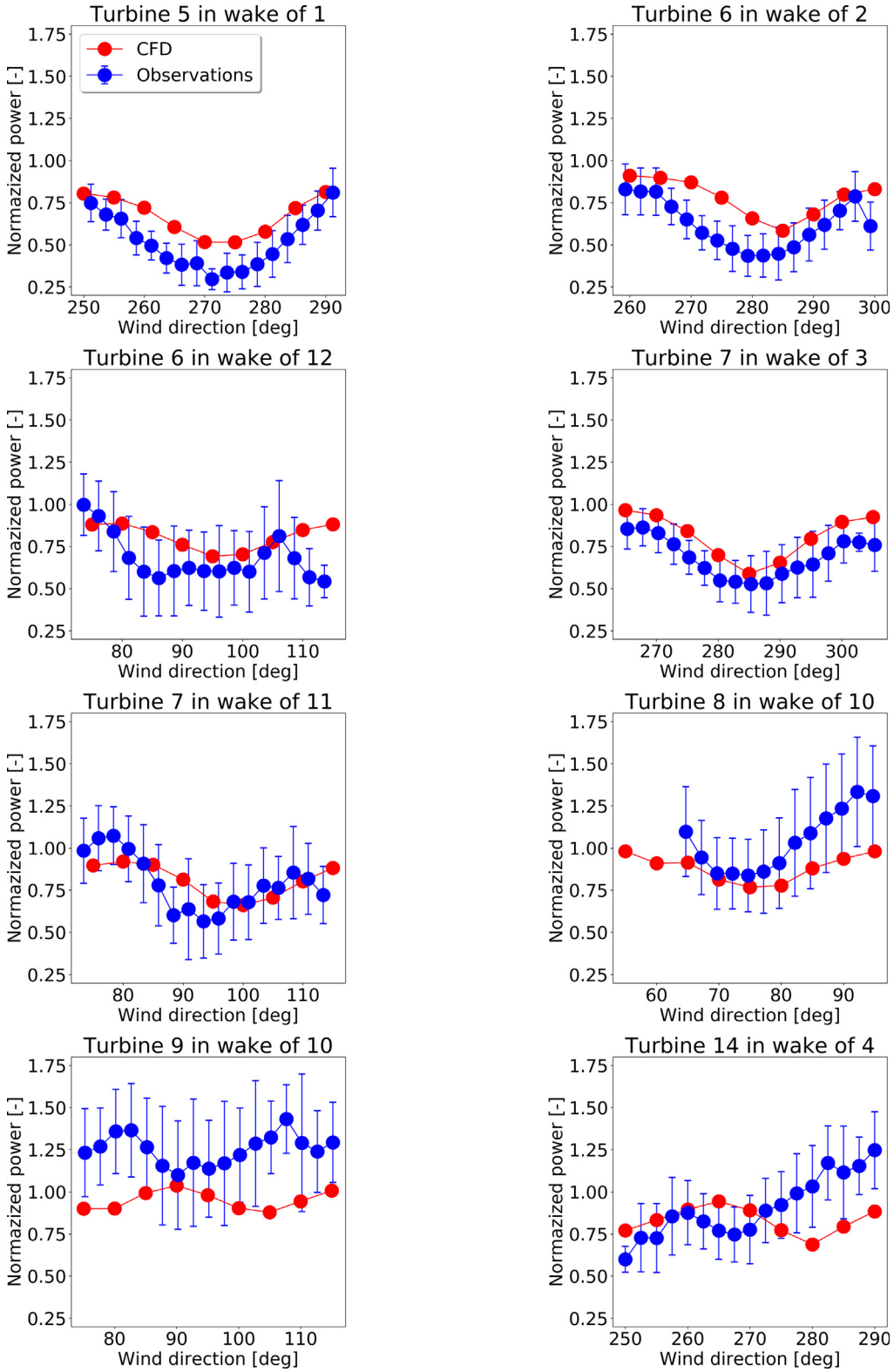

Fig. 5. Normalized power of wind turbines operating in wake conditions. The plots show the experimental data along with one standard deviation (blue) and the CFD predictions (red). (For interpretation of the references to colour in this figure legend, the reader is referred to the web version of this article.)

was instead assumed to comprise six equally-weighted wind directions with a constant wind speed of 10 m/s.

The layouts resulting from the optimization are shown in Fig. 9 and 10 for a regular and a random initial layout, respectively. The quantity of interest considered for the optimization is the normalized AEP, which is the ratio between the actual AEP and the AEP that would be generated by the same turbines operating in isolation (i.e., without wake effects) on a flat terrain. Resulting values of the normalized AEP for the cases considered are reported in Table 3. Convergence was reached within 10 (or fewer) iterations of the optimization process for all the cases analyzed.

When a regular initial layout was used, we notice that the resulting

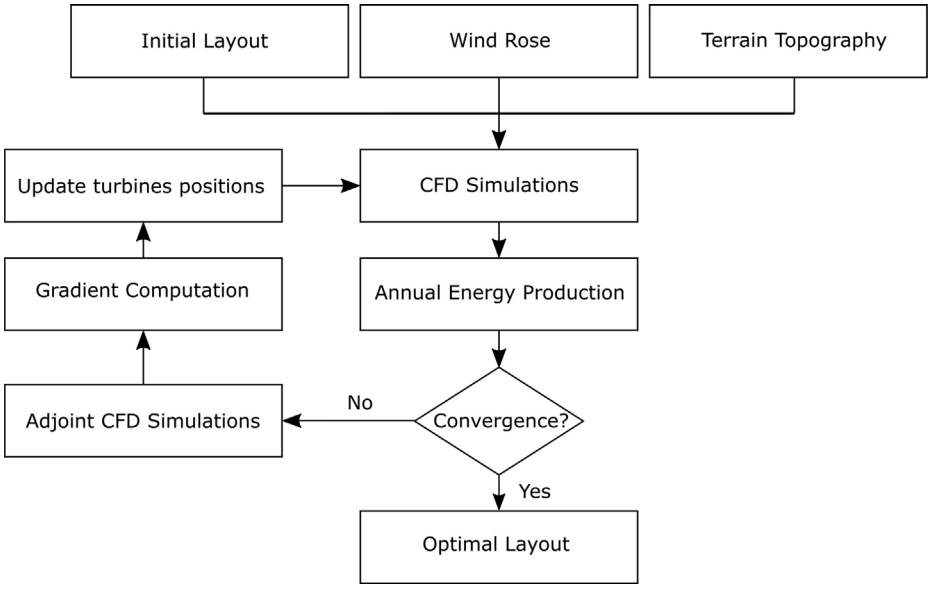

Fig. 6. Flow chart reproducing the optimization methodology used to solve the wind farm layout optimization problem in complex terrain.

optimal layouts retained a clear regularity, which can be explained by the symmetry of both the wind rose and the initial layout. The layouts were, in fact, symmetric about a horizontal or vertical line passing by the center of the domain. These symmetric optimal layouts obtained when using equally-weighted wind directions with a constant wind speed are usually considered evidence of an effective optimization process [49].

Differences can be highlighted between 2D and 3D results for a flat terrain scenario. It is possible to notice that even if the layouts look quite similar, the turbines in the 2D cases are further apart. This can be explained by the different modeling implementation of the wind turbines. Whereas the 3D case used actual cylinders to model the wind turbines, in the 2D case the actual turbine volumes were rectangular prisms with unit height and rectangular base with width equal to the rotor diameter. Because of this, the 2D modeling inherently generates wake effects that are higher and therefore induces the optimization to move the turbines further apart.

The normalized AEP of the optimal layouts resulted greater than one in some cases. This means that the actual AEP was greater than the one that would be generated by the same turbines operating in isolation and on a flat terrain. For instance, this occurred in the 2D case with a regular initial layout. The reason for this result lies in the fact that the CFD models can accurately resolve the entire flow field and capture the local speed-up effect surrounding the turbine rotor just outside of the wake regions. The optimization algorithm exploited this feature and moved the turbines toward these favorable regions where speedups are expected to be larger. Although the optimal layouts of the 3D cases in flat terrain were very similar to the 2D cases, the AEP results of the former ones did not clearly show to benefit from this flow characteristic. As also suggested in previous studies [49], this indicates that speed-up effects generated by the turbine presence are more pronounced in 2D simulations. A value of normalized AEP greater than one was observed also for the 3D cases in complex terrain. This can be explained by the fact that the Gaussian-shaped hill induced a speed-up effect above it that increased the available kinetic energy that can be captured by the turbines. A consequence of this effect can be seen in the optimal layout for the 3D case in complex terrain with a random initial layout (see Fig. 10c). In fact, differently from the other two cases with the same initial layout, one of the turbines remains in the middle of the domain on top of the hill where the speedup and therefore the energy increase are expected to be maximum.

5.2. Nygårdsfjellet wind farm

For the Nygårdsfjellet wind farm, we used the same domain and set-up of the validation process and we imposed a circular constraint of 7.5 D radius, as shown in Fig. 12, and a minimum distance of 1 D between any two turbines. For this optimization, we used as starting configuration only the original layout of the wind farm without considering any other hypothetical case. A simplification was introduced for the wind rose that characterizes the wind resource of the site. The original wind rose [61], shown in Fig. 11a, is divided in 36 bins for the wind direction and 5 for the wind speed, which results in a total of 180 wind states. To calculate the AEP of the farm, a CFD simulation should be run for each of the wind states. We however deemed necessary a reduction of these wind states to complete the optimization process. We simplified

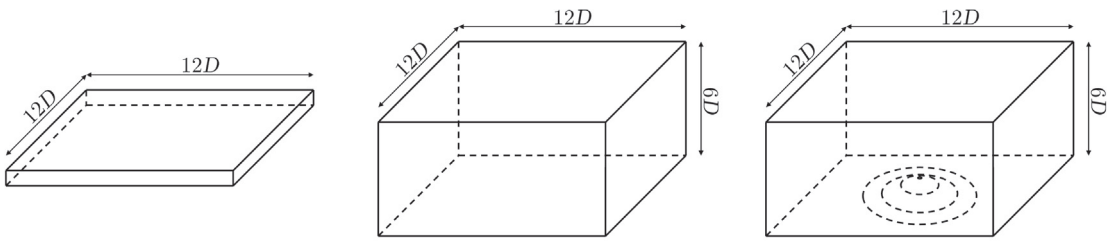

(a) 2D case, flat terrain (b) 3D case, flat terrain (c) 3D case, complex terrain

Fig. 7. Illustration of the domains used for the application of the 2D [26] and 3D (this work) methodologies for the idealized wind farm.

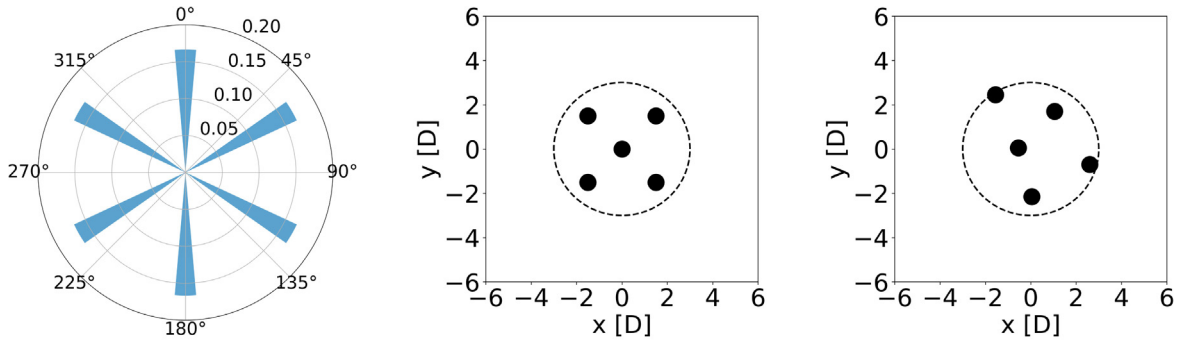

(a) Wind rose (b) Regular initial layout (c) Random initial layout

Fig. 8. Wind rose and initial layouts used for the optimization process of the idealized wind farm.

the wind rose to the one shown in Fig. 11b, which resembles the original and preserves the predominant east–west directionality of the wind resource. The simplified wind rose has two wind states with uniform wind speed of 9 m/s and wind directions of 95° and 280° with probability of occurrence of 0.646 and 0.354, respectively.

The initial and final layouts resulting from the optimization are reported in Fig. 12 where we also show the normalized average power production of each of the turbines. Fig. 13 shows instead a more detailed comparison of the initial and optimal layouts by highlighting the movement of each turbine. The optimization stopped and convergence was reached after 14 iterations of the optimization process. The AEP of the farm with the optimal layout was increased by 6.6% with respect to the original configuration by moving the turbines at most 266 m and 111 m on average. The overall computational time was approximately 600 core-hours, roughly 5 days given our computational resources.

By taking a closer look to the results, some important observations can be made. First, turbines that originally had some of the lowest average power productions, namely, 1, 6, and 7, reported a significant improvement. Turbines 6 and 7, even though their movement was minimal, benefited from the movement of the east-side upstream turbines 10, 11, 12, and 13 toward south-east. This resulted in a higher wind potential available to the turbines in the center of the domain. On the other hand, turbine 5, which was also in the group of turbines whose performance was affected the most, did not show any significant improvement itself but its movement increased the power production of turbine 1, downstream for easterly winds. It is clear that all the turbines were moved in a coordinated manner to increase the overall annual energy production. To note is also the fact that the circular constraint set in the optimization process prevented any further movement apart of the turbines. In fact, Turbines 8 and 14, which were originally outside of the circular constraint were forced inside by the optimization algorithm, which may have capped the AEP improvement realized by the optimization algorithm.

Overall, the presented optimization methodology effectively improved the AEP of the wind farms in complex terrain by changing their turbine positions. This was enabled by both (a) the use of an experimentally-validated, full-scale, 3D, turbulent CFD model that, as opposed to traditionally-used engineering models, could solve and capture turbine- and terrain-induced flow features, and their mutual interaction; and (b) the use of a continuous formulation of the adjoint method to compute the gradients of the AEP with respect to changes in the turbine positions along directions that are locally tangential to the terrain profile. As a consequence, the optimizer could exploit optimal locations that would have not been otherwise found. With a small wind farm (<10 turbines), in an idealized scenario with a single smooth terrain feature, the improvements in AEP ranged from about 3 to 6% depending of the initial layout and terrain geometry. Given the simplified problem, we could understand how heuristics, such as speedups around turbines and terrain features, played a crucial role in determining the optimal siting of turbines and increasing the AEP. With the application to a real wind farm with 14 turbines, the AEP improved more that 6% with respect to the initial, currently operational turbine layout, which was presumably designed and built giving at least some consideration to energy production optimality.

6. Conclusions

In the present work, we developed and applied a gradient-based optimization methodology for wind farms in both flat and complex terrains. This methodology integrates the high accuracy and flexibility of the CFD models and uses the adjoint method to calculate the required gradients. As opposed to previous studies, this methodology is general in its formulation and can handle different wind farm configurations, wind resource distributions and, more importantly, terrain topography.

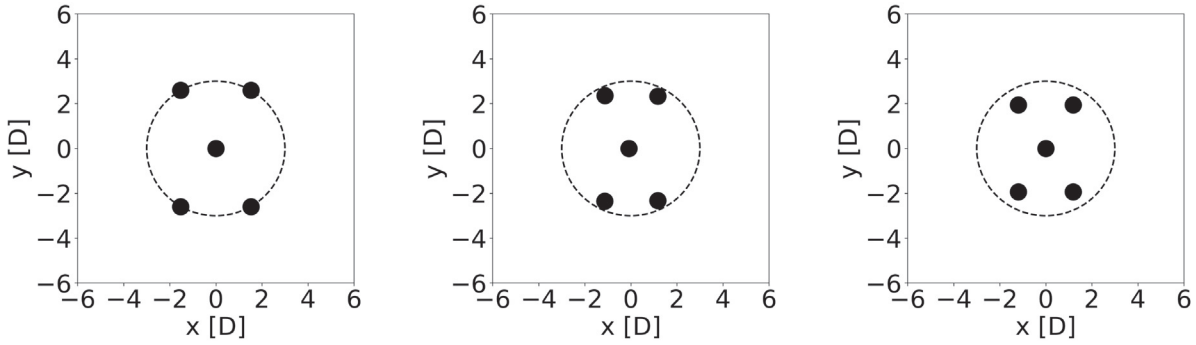

(a) 2D case, flat terrain (b) 3D case, flat terrain (c) 3D case, complex terrain

Fig. 9. Optimal layouts resulting from the optimization process of the idealized wind farm starting from a regular initial layout.

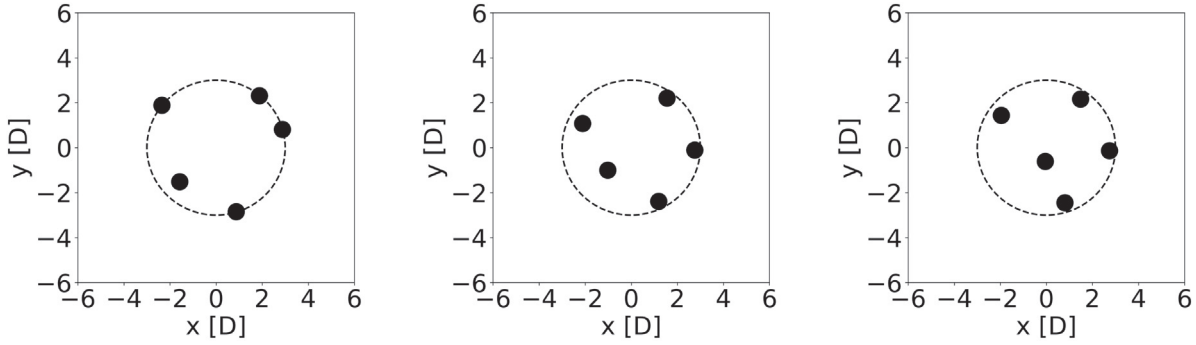

(a) 2D case, flat terrain (b) 3D case, flat terrain (c) 3D case, complex terrain

Fig. 10. Optimal layouts resulting from the optimization process of the idealized wind farm starting from a random initial layout.

Table 3
Normalized AEP and improvement with respect to the initial layout resulting from the optimization of the idealized wind farm. Values are reported for each of the initial layouts and for each of the cases tested.

	Regular initial layout		Random initial layout	
	Norm. AEP	Impr. [%]	Norm. AEP	Impr. [%]
2D case, flat terrain	1.032	13.9	0.982	6.0
3D case, flat terrain	0.972	6.1	0.964	2.8
3D case, complex terrain	1.013	3.0	1.019	3.2

The adjoint method was verified on an idealized 2-turbine scenario where only the gradient of the wind turbine operating in wake conditions was evaluated. The gradients predicted by the adjoint method were generally accurate when compared to a central difference discretization approach. We showed how the adjoint method can significantly reduce the computational time for gradient computations in high-dimensional optimization of very large control spaces, a feature that enabled the proposed CFD-based WFLO. The CFD model based on RANS equations was validated against the observed power production data of the Nygårdsfjellet wind farm. These data were from turbines operating in wake conditions and on complex terrain. The CFD model was able to provide good predictions of the power production for most of the cases considered, though discrepancies were observed in a few of them. The validation also highlighted the challenge of simulating wind farms in complex terrains, for which boundary conditions are uncertain as a consequence of the larger scale atmospheric flows and local weather patterns that influence the flow conditions at the wind farm.

The optimization methodology was applied and tested on two wind farms in complex terrain, namely, an idealized wind farm consisting of 5 wind turbines and the Nygårdsfjellet wind farm with 14 turbines. The idealized wind farm provided useful heuristics for checking optimization results, such as the siting of turbines in higher wind potential regions around turbines and terrain features, and the effect of initial layouts on the resulting (locally) optimal AEP. For the optimization of the Nygårdsfjellet wind farm, we instead used the original, currently operational layout as a starting point. We observe that the optimization methodology for wind farms in complex terrains could effectively improve the AEP of the farms by changing their turbine positions. With the idealized wind farm, the improvements ranged from about 3 to 6% depending of the initial layout and terrain geometry, whereas with real wind farm, the AEP was improved by more that 6%. This was, in fact, the first fully CFD-based methodology being applied to the wind farm layout optimization in complex terrain. As opposed to the state of the art in WFLO, we showed that this methodology is capable of accurately simulating both turbine wakes and terrain-induced flow features and optimally designing turbine layouts in a way that approximate or simplified models could not provide. We also demonstrated that this innovative methodology is feasible with current computational resources, and an optimization process can be completed within days.

We deem that the availability of a comprehensive optimization model for wind farms in complex terrains and an efficient algorithm for its solution will enable the evaluation of optimal turbine sites in areas previously unexplored and will ultimately reduce design and development costs for new on-shore wind farms. The developed framework, although based on some simplifications to facilitate the computational tractability of the problem, could be extended and improved to include other aspects of the wind farm design. These include using different hub heights or different turbines to further exploit terrain features, introducing land availability constraints, and considering environmentally-related setbacks such as buffer zones around rivers, forests or human dwellings, among others. On the modelling side, different turbulence closures for the RANS equations could be

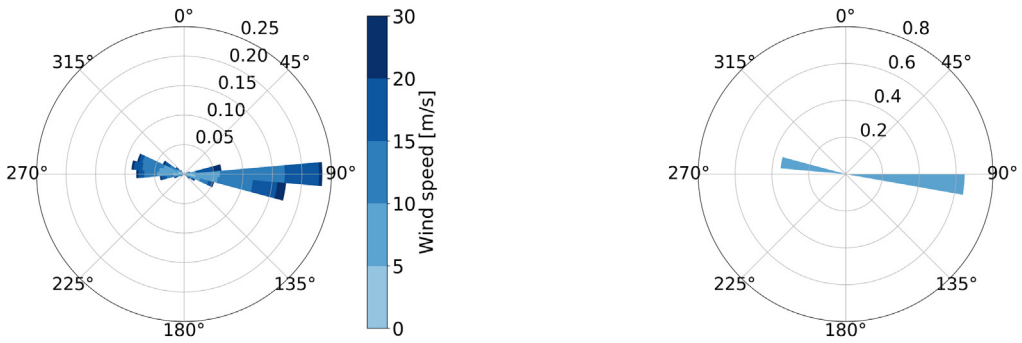

(a) Original wind rose [61] (b) Simplified wind rose

Fig. 11. Original and simplified wind roses for the optimization of the Nygårdsfjellet wind farm.

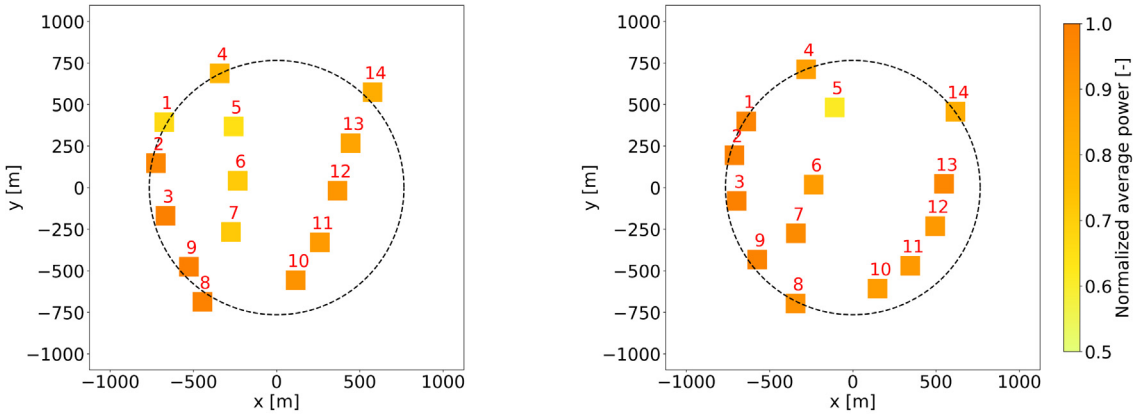

(a) Initial layout (b) Optimal layout

Fig. 12. Initial and optimal layout resulting from the optimization process of the Nygårdsfjellet wind farm. Colour indicates the normalized average power for each of the turbines. (For interpretation of the references to colour in this figure legend, the reader is referred to the web version of this article.)

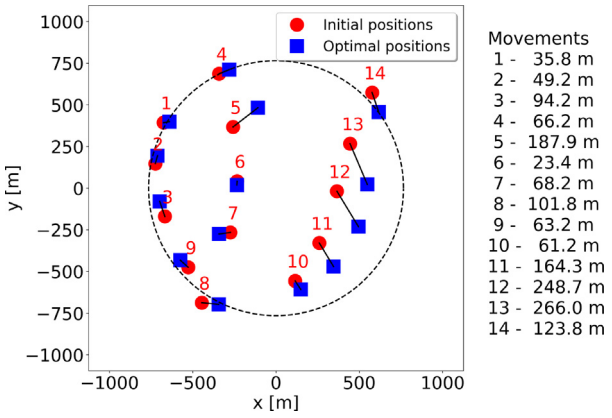

Fig. 13. Comparison between the initial and optimal layout resulting from the optimization process of the Nygårdsfjellet wind farm. Turbine movements are indicated by the black lines and the corresponding distances are reported on the right of the figure.

implemented and their impact investigated. Also, the CFD predictions, and consequently the optimization results, would benefit if wind and atmospheric conditions as well as site and turbine geometry were known with lower uncertainties. Lastly, on the economic side, more comprehensive cost functions that include other aspects of the design process such as electrical interconnections and civil engineering infrastructures could be considered. The integration of all these aspects would create a multi-disciplinary optimization framework that could provide optimal layout designs that minimize the wind farm LCOE while meeting environmental regulations and other site constraints.

Code availability

The code developed and used in the present study for the wind farm layout optimization is available in the GitHub repository at https://github.com/eantonini/CFD-based-WFLO.

CRediT authorship contribution statement

Enrico G.A. Antonini: Conceptualization, Data curation, Formal analysis, Investigation, Methodology, Project administration, Software, Validation, Visualization, Writing - original draft, Writing - review & editing. **David A. Romero:** Conceptualization, Formal analysis, Project administration, Resources, Software, Supervision, Writing - original draft, Writing - review & editing. **Cristina H. Amon:** Conceptualization, Formal analysis, Funding acquisition, Project administration, Supervision, Writing - review & editing.

Declaration of Competing Interest

The authors declare that they have no known competing financial interests or personal relationships that could have appeared to influence the work reported in this paper.

Acknowledgments

Computations were performed on the Niagara supercomputer at the SciNet HPC Consortium [65,66]. SciNet is funded by: the Canada Foundation for Innovation under the auspices of Compute Canada; the Government of Ontario; Ontario Research Fund - Research Excellence; and the University of Toronto.

References

[1] Barthelmie RJ, Hansen KS, Frandsen ST, Rathmann O, Schepers JG, Schlez W, et al. Modelling and measuring flow and wind turbine wakes in large wind farms offshore. Wind Energy 2009;12(5):431–44. https://doi.org/10.1002/we.348.
[2] Herbert-Acero JF, Probst O, Réthoré P-E, Larsen GC, Castillo-Villar KK. A review of methodological approaches for the design and optimization of wind farms. Energies 2014;7(11):6930–7016. https://doi.org/10.3390/en7116930.
[3] Serrano González J, Burgos Payán M, Riquelme Santos JM, González-Longatt F. A review and recent developments in the optimal wind-turbine micro-siting problem. Renew Sustain Energy Rev 2014;30:133–44. https://doi.org/10.1016/j.rser.2013.09.027.
[4] Yamani Douzi Sorkhabi S, Romero DA, Yan GK, Gu MD, Moran J, Morgenroth M, et al. The impact of land use constraints in multi-objective energy-noise wind farm layout optimization. Renewable Energy 2016;85:359–70. https://doi.org/10.1016/j.renene.2015.06.026.
[5] Waye KP, Öhrström E. Psycho-acoustic characters of relevance for annoyance of wind turbine noise. J Sound Vib 2002;250(1):65–73. https://doi.org/10.1006/jsvi.2001.3905.
[6] Saidur R, Rahim NA, Islam MR, Solangi KH. Environmental impact of wind energy. Renew Sustain Energy Rev 2011;15(5):2423–30. https://doi.org/10.1016/j.rser.2011.02.024.
[7] Yin Kwong W, Zhang PY, Romero DA, Moran J, Morgenroth M, Amon CH. Multi-objective wind farm layout optimization considering energy generation and noise propagation with NSGA-II. J Mech Des 2014;136(9):091010. https://doi.org/10.1115/1.4027847.
[8] Politis ES, Prospathopoulos JM, Cabezón D, Hansen KS, Chaviaropoulos PK, Barthelmie RJ. Modeling wake effects in large wind farms in complex terrain: the problem, the methods and the issues. Wind Energy 2012;15(1):161–82. https://doi.org/10.1002/we.481.
[9] Mattuella JML, Loredo-Souza AM, Oliveira MGK, Petry AP. Wind tunnel experimental analysis of a complex terrain micrositing. Renew Sustain Energy Rev 2016;54:110–9. https://doi.org/10.1016/j.rser.2015.09.088.
[10] Røkenes K, Krogstad P. Wind tunnel simulation of terrain effects on wind farm siting. Wind Energy 2009;12:391–410. https://doi.org/10.1002/we.310.
[11] Castellani F, Astolfi D, Burlando M, Terzi L. Numerical modelling for wind farm

operational assessment in complex terrain. J Wind Eng Ind Aerodyn 2015;147:320–9. https://doi.org/10.1016/j.jweia.2015.07.016.
[12] Castellani F, Astolfi D, Mana M, Piccioni E, Becchetti M, Terzi L. Investigation of terrain and wake effects on the performance of wind farms in complex terrain using numerical and experimental data. Wind Energy 2017;20(7):1277–89. https://doi.org/10.1002/we.2094.
[13] Astolfi D, Castellani F, Terzi L. A study of wind turbine wakes in complex terrain through RANS simulation and SCADA data. J Sol Energy Eng 2018;140(3):031001. https://doi.org/10.1115/1.4039093.
[14] Murali A, Rajagopalan RG. Numerical simulation of multiple interacting wind turbines on a complex terrain. J Wind Eng Ind Aerodyn 2017;162:57–72. https://doi.org/10.1016/j.jweia.2017.01.005.
[15] Makridis A, Chick J. Validation of a CFD model of wind turbine wakes with terrain effects. J Wind Eng Ind Aerodyn 2013;123:12–29. https://doi.org/10.1016/j.jweia.2013.08.009.
[16] Vermeer LJ, Sørensen JN, Crespo A. Wind turbine wake aerodynamics. Prog Aerosp Sci 2003;39(6–7):467–510. https://doi.org/10.1016/S0376-0421(03)00078-2.
[17] Jensen NO. A note on wind generator interaction. Tech. rep. Roskilde, Denmark: Risø National Laboratory; 1983.
[18] Frandsen ST, Barthelmie RJ, Pryor SC, Rathmann O, Larsen S, Højstrup J, et al. Analytical modelling of wind speed deficit in large offshore wind farms. Wind Energy 2006;9(1–2):39–53. https://doi.org/10.1002/we.189.
[19] Larsen GC. A simple wake calculation procedure. Tech. rep. Roskilde, Denmark: Risø National Laboratory; 1988.
[20] Katic I, Hojstrup J, Jensen NO. A simple model for cluster efficiency. Proceedings of the European Wind Energy Conference and Exhibition, Rome, Italy. 1986.
[21] Kuo JY, Romero DA, Amon CH. A mechanistic semi-empirical wake interaction model for wind farm layout optimization. Energy 2015;93:2157–65. https://doi.org/10.1016/j.energy.2015.10.009.
[22] Sanderse B, van der Pijl SP, Koren B. Review of computational fluid dynamics for wind turbine wake aerodynamics. Wind Energy 2011;14(7):799–819. https://doi.org/10.1002/we.458.
[23] Crespo A, Hernández J, Frandsen ST. Survey of modelling methods for wind turbine wakes and wind farms. Wind Energy 1999;2(1):1–24. https://doi.org/10.1002/(SICI)1099-1824(199901/03)2:1<1::AID-WE16>3.0.CO;2-7.
[24] Cabezón D, Migoya E, Crespo A. Comparison of turbulence models for the computational fluid dynamics simulation of wind turbine wakes in the atmospheric boundary layer. Wind Energy 2011;14(7):909–21. https://doi.org/10.1002/we.516.
[25] Antonini EGA, Romero DA, Amon CH. Analysis and modifications of turbulence models for wind turbine wake simulations in atmospheric boundary layers. In: ASME international mechanical engineering congress and exposition, vol. 6B, Phoenix, Arizona, USA: ASME; 2016, p. V06BT08A062. https://doi.org/10.1115/IMECE2016-67353. http://proceedings.asmedigitalcollection.asme.org/proceeding.aspx?doi=10.1115/IMECE2016-67353.
[26] Antonini EGA, Romero DA, Amon CH. Analysis and modifications of turbulence models for wind turbine wake simulations in atmospheric boundary layers. J Sol Energy Eng 2018;140(3):031007. https://doi.org/10.1115/1.4039377.
[27] Antonini EGA, Romero DA, Amon CH. Improving CFD Wind Farm Simulations incorporating Wind Direction Uncertainty. Renewable Energy 2019;133:1011–23. https://doi.org/10.1016/j.renene.2018.10.084.
[28] Mehta D, van Zuijlen AH, Koren B, Holierhoek JG, Bijl H. Large eddy simulation of wind farm aerodynamics: a review. J Wind Eng Ind Aerodyn 2014;133:1–17. https://doi.org/10.1016/j.jweia.2014.07.002.
[29] Shakoor R, Hassan MY, Raheem A, Wu YK. Wake effect modeling: A review of wind farm layout optimization using Jensen's model. Renew Sustain Energy Rev 2016;58:1048–59. https://doi.org/10.1016/j.rser.2015.12.229.
[30] Mosetti G, Poloni C, Diviacco D. Optimization of wind turbine positioning in large wind farms by means of a genetic algorithm. J Wind Eng Ind Aerodyn 1994;51(1):105–16. https://doi.org/10.1016/0167-6105(94)90080-9.
[31] Grady SA, Hussaini MY, Abdullah MM. Placement of wind turbines using genetic algorithms. Renewable Energy 2005;30(2):259–70. https://doi.org/10.1016/j.renene.2004.05.007.
[32] Kusiak A, Song Z. Design of wind farm layout for maximum wind energy capture. Renewable Energy 2010;35(3):685–94. https://doi.org/10.1016/j.renene.2009.08.019.
[33] Serrano González J, Gonzalez Rodriguez AG, Castro Mora J, Riquelme Santos JM, Burgos Payán M. Optimization of wind farm turbines layout using an evolutive algorithm. Renewable Energy 2010;35(8):1671–81. https://doi.org/10.1016/j.renene.2010.01.010.
[34] Emami A, Noghreh P. New approach on optimization in placement of wind turbines within wind farm by genetic algorithms. Renewable Energy 2010;35(7):1559–64. https://doi.org/10.1016/j.renene.2009.11.026.
[35] Bilbao M, Alba E. Simulated annealing for optimization of wind farm annual profit. Proocedings of the 2nd International Symposium on Logistics and Industrial Informatics, Linz, Austria 2009. p. 1–5. https://doi.org/10.1109/LINDI.2009.5258656.
[36] Chowdhury S, Zhang J, Messac A, Castillo L. Unrestricted wind farm layout optimization (UWFLO): Investigating key factors influencing the maximum power generation. Renewable Energy 2012;38(1):16–30. https://doi.org/10.1016/j.renene.2011.06.033.
[37] Pookpunt S, Ongsakul W. Optimal placement of wind turbines within wind farm using binary particle swarm optimization with time-varying acceleration coefficients. Renewable Energy 2013;55:266–76. https://doi.org/10.1016/j.renene.2012.12.005.
[38] Hou P, Hu W, Soltani M, Chen Z. Optimized placement of wind turbines in large-scale offshore wind farm using particle swarm optimization algorithm. IEEE Trans Sustainable Energy 2015;6(4):1272–82. https://doi.org/10.1109/TSTE.2015.2429912.
[39] Hou P, Hu W, Chen C, Soltani M, Chen Z. Optimization of offshore wind farm layout in restricted zones. Energy 2016;113:487–96. https://doi.org/10.1016/j.energy.2016.07.062.
[40] Hou P, Hu W, Soltani M, Chen C, Chen Z. Combined optimization for offshore wind turbine micro siting. Appl Energy 2017;189:271–82. https://doi.org/10.1016/j.apenergy.2016.11.083.
[41] Ozturk UA, Norman BA. Heuristic methods for wind energy conversion system positioning. Electric Power Syst Res 2004;70(3):179–85. https://doi.org/10.1016/j.epsr.2003.12.006.
[42] Turner SDO, Romero DA, Zhang PY, Amon CH, Chan TCY. A new mathematical programming approach to optimize wind farm layouts. Renewable Energy 2014;63:674–80. https://doi.org/10.1016/j.renene.2013.10.023.
[43] Feng J, Shen WZ. Solving the wind farm layout optimization problem using random search algorithm. Renewable Energy 2015;78:182–92. https://doi.org/10.1016/j.renene.2015.01.005.
[44] Du Pont BL, Cagan J. An extended pattern search approach to wind farm layout optimization. J Mech Des 2012;134(8):081002. https://doi.org/10.1115/1.4006997.
[45] Pérez B, Mínguez R, Guanche R. Offshore wind farm layout optimization using mathematical programming techniques. Renewable Energy 2013;53:389–99. https://doi.org/10.1016/j.renene.2012.12.007.
[46] Guirguis D, Romero DA, Amon CH. Toward efficient optimization of wind farm layouts: Utilizing exact gradient information. Appl Energy 2016;179:110–23. https://doi.org/10.1016/j.apenergy.2016.06.101.
[47] Giles MB, Pierce NA. An introdountion to the adjoint approach to design. Flow Turbulence Combust 2000;65(3–4):393–415. https://doi.org/10.1023/a:1011430410075.
[48] King RN, Hamlington PE, Dykes K, Graf P. Adjoint optimization of wind farm layouts for systems engineering analysis. In: Proceedings of the 34th wind energy symposium; 2016. https://doi.org/10.2514/6.2016-2199.
[49] King RN, Dykes K, Graf P, Hamlington PE. Optimization of wind plant layouts using an adjoint approach. Wind Energy Sci 2017;2(1):115–31. https://doi.org/10.5194/wes-2-115-2017.
[50] Antonini EGA, Romero DA, Amon CH. Continuous adjoint formulation for wind farm layout optimization: A 2D implementation. Appl Energy 2018;228:2333–45. https://doi.org/10.1016/j.apenergy.2018.07.076.
[51] Kuo JY, Romero DA, Beck JC, Amon CH. Wind farm layout optimization on complex terrains – Integrating a CFD wake model with mixed-integer programming. Appl Energy 2016;178:404–14. https://doi.org/10.1016/j.apenergy.2016.06.085.
[52] Feng J, Shen W, Li Y. An optimization framework for wind farm design in complex terrain. Appl Sci 2018;8(11):2053. https://doi.org/10.3390/app8112053.
[53] Jameson A. Aerodynamic design via control theory. Sci Comput 1988;3(3):233–60. https://doi.org/10.1007/BF01061285.
[54] Anderson WK, Venkatakrishnan V. Aerodynamic design optimization on unstructured grids with a continuous adjoint formulation. Comput Fluids 1999;28(4–5):443–80. https://doi.org/10.1016/S0045-7930(98)00041-3.
[55] Papadimitriou DI, Giannakoglou KC. A continuous adjoint method with objective function derivatives based on boundary integrals, for inviscid and viscous flows. Comput Fluids 2007;36(2):325–41. https://doi.org/10.1016/j.compfluid.2005.11.006.
[56] Dwight RP, Brezillon J. Effect of approximations of the discrete adjoint on gradient-based optimization. AIAA J 2006;44(12):3022–31. https://doi.org/10.2514/1.21744.
[57] Castro C, Lozano C, Palacios F, Zuazua E. Systematic continuous adjoint approach to viscous aerodynamic design on unstructured grids. AIAA J 2007;45(9):2125–39. https://doi.org/10.2514/1.24859.
[58] The OpenFOAM Foundation Ltd, OpenFOAM 5.0, http://www.openfoam.org/, accessed: June 2018.
[59] Prospathopoulos JM, Politis ES, Rados KG, Chaviaropoulos PK. Evaluation of the effects of turbulence model enhancements on wind turbine wake predictions. Wind Energy 2011;14(2):285–300. https://doi.org/10.1002/we.419.
[60] van der Laan MP, Sørensen NN, Réthoré P-E, Mann J, Kelly MC, Troldborg N, et al. An improved k-∈model applied to a wind turbine wake in atmospheric turbulence. Wind Energy 2015;18(5):889–907. https://doi.org/10.1002/we.1736.
[61] Seim F, Gravdahl AR, Adaramola MS. Validation of kinematic wind turbine wake models in complex terrain using actual windfarm production data. Energy 2017;123:742–53. https://doi.org/10.1016/j.energy.2017.01.140.
[62] Wilcox DC. Reassessment of the scale-determining equation for advanced turbulence models. AIAA J 1988;26(11):1299–310. https://doi.org/10.2514/3.10041.
[63] Kraft D. A software package for sequential quadratic programming. Tech. rep. Oberpfaffenhofen, Germany: Institut für Dynamik der Flugsysteme; 1988.
[64] Johnson SG. The NLopt nonlinear-optimization package, http://ab-initio.mit.edu/nlopt, accessed: June 2016.
[65] Loken C, Gruner D, Groer L, Peltier R, Bunn N, et al. SciNet: Lessons learned from building a power-efficient top-20 system and data centre. J Phys: Conf Ser 2010;256(1). https://doi.org/10.1088/1742-6596/256/1/012026.
[66] Ponce M, van Zon R, Northrup S, Gruner D, Chen J, Ertinaz F, et al. Deploying a Top-100 supercomputer for large parallel workloads: the niagara supercomputer. Proceedings of the Practice and Experience in Advanced Research Computing, Chicago, IL, USA 2019. https://doi.org/10.1145/3332186.3332195.